NANO LETTERS

2003
Vol. 3, No. 5
597−602

Carbon Nanotube Nanoelectrode Array for Ultrasensitive DNA Detection

Jun Li,*,† Hou Tee Ng,† Alan Cassell,† Wendy Fan,† Hua Chen,† Qi Ye,† Jessica Koehne, Jie Han,† and M. Meyyappan

NASA Ames Research Center, Moffett Field, California 94035

Received February 5, 2003; Revised Manuscript Received March 4, 2003

ABSTRACT

A nanoelectrode array based on vertically aligned multiwalled carbon nanotubes (MWNTs) embedded in SiO_2 is used for ultrasensitive DNA detection. Characteristic electrochemical behaviors are observed for measuring bulk and surface-immobilized redox species. Sensitivity is dramatically improved by lowering the nanotube density. Oligonucleotide probes are selectively functionalized to the open ends of nanotubes. The hybridization of subattomole DNA targets can be detected by combining such electrodes with $Ru(bpy)_3^{2+}$ mediated guanine oxidation.

The quick and reliable detection of small amounts of DNA/RNA has become increasingly important in molecular diagnosis. Extremely sensitive yet inexpensive and robust detection methods which do not require extensive sample pretreatment and derivatization are essential for the efficient use of genomic information. Electrochemical (EC) techniques have shown great potential in providing viable solutions to this challenge.[1] Individually addressable microelectrode arrays have been demonstrated for molecular diagnosis[2−4] which can be directly integrated with microelectronics and microfluidics systems to gain advantages in miniaturization and multiplex detection. In addition, nanoscale sensing elements can be incorporated to seek ultrahigh sensitivity. We demonstrate here that nanoelectrodes, particularly a carbon nanotube (CNT) based nanoelectrode array, can be integrated into a EC system for ultrasensitive chemical and DNA detection. The nanoelectrode array is fabricated with a bottom-up scheme resulting in precisely positioned and well aligned multiwalled carbon nanotube (MWNT) array embedded in a planarized SiO_2 matrix.[5,6] The open ends of MWNTs exposed at the dielectric surface act as nanoelectrodes. The well-defined graphitic chemistry allows us to selectively functionalize the nanotube ends with primary amine-terminated oligonucleotide probes. Combining the CNT nanoelectrode array with $Ru(bpy)_3^{2+}$ mediated guanine oxidation method,[7] the hybridization of less than a few attomoles of oligonucleotide targets can be easily detected, showing orders of magnitude improvement in sensitivity comparing to previous EC studies of DNA immobilized using self-assembled monolayers.[3,4,8]

The performance of electrodes with respect to speed and spatial resolution is known to scale inversely with the electrode radius.[9−11] It is of interest for biosensing to reduce the radius of electrodes to 10−100 nm, approaching the size of biomolecules. However, results from such systems are rare due to the lack of reliable fabrication and heterogeneous integration methods. CNTs, particularly MWNTs, with well-defined nanoscale geometry, are attractive nanoelectrode materials. They are expected to present a wide electrochemical window, flexible surface chemistry, and biocompatibility, similar to other widely used carbon electrodes. The open end of a MWNT is expected to show a fast electron transfer rate (ETR) similar to the graphite edge-plane electrode while the sidewall is inert like the graphite basal-plane.[12] Fast ETR is demonstrated along the tube axis.[13,14] Such MWNT electrode could interrogate target species, down to single molecule level, at one end and sustain electron transport along the tube axis to the measuring circuit with minimum interference from the environment. This concept requires aligned and well-insulated MWNTs. While a single nanoelectrode can provide the desired temporal and spatial advantages, we are motivated to develop an array of nanoelectrodes for analytical applications requiring reliable statistics and multiplex detection.

Figure 1a,b shows scanning electron microscope (SEM) images of a 3 × 3 array of individually addressed electrodes on a Si(100) wafer covered with 500 nm thermal oxide. The electrodes and contact lines are 200 nm thick Cr patterned with UV-lithography. Each electrode can be varied from 2 × 2 to 200 × 200 μm^2, consisting of a vertically aligned MWNT array grown by plasma-enhanced chemical vapor deposition (PECVD) from 10 to 20 nm thick Ni catalyst films. Figure 1c,d shows MWNT arrays grown on 2 μm and 200 nm diameter Ni spots defined by UV and e-beam lithography, respectively. The spacing and spot size can be precisely controlled. The diameter of the MWNTs is uniform over the whole chip and can be controlled between 30 and

* Corresponding author: Phone (650) 604-6459, Fax (650) 604-5244, E-mail jli@mail.arc.nasa.gov.
† Also at ELORET Corporation.

10.1021/nl0340677 CCC: $25.00
Published on Web 03/22/2003

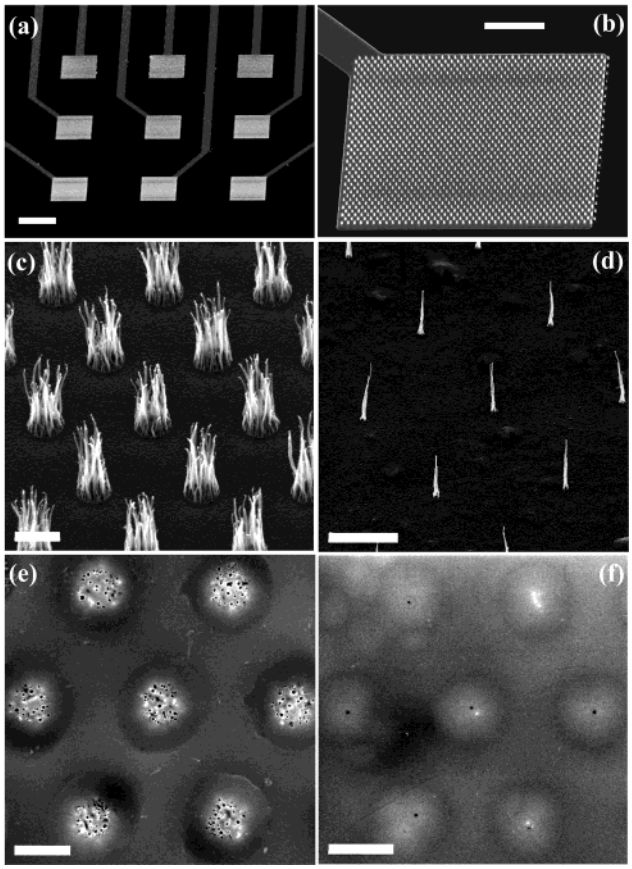

Figure 1. SEM images of (a) 3 × 3 electrode array, (b) array of MWNT bundles on one of the electrode pads, (c) and (d) array of MWNTs at UV-lithography and e-beam patterned Ni spots, respectively, (e) and (f) the surface of polished MWNT array electrodes grown on 2 μm and 200 nm spots, respectively. Panels (a−d) are 45° perspective views and panels (e−f) are top views. The scale bars are 200, 50, 2, 5, 2, and 2 μm, respectively.

100 nm by PECVD conditions. The number of CNTs at each spot can be varied as well by changing the thickness of the Ni film. Single nanotubes can be grown at each catalyst spot if their size is reduced below 100 nm. We use a tetraethoxysilane CVD process to encapsulate each nanotube and the substrate surface with a conformal SiO_2 film, resulting in a mechanically stable and well-insulated matrix, followed with chemical mechanical polishing for planarization and exposing the very ends of the CNTs.

Figure 1e,f shows the embedded CNT array electrodes with different patterns after polishing. Clearly, CNTs retain their integrity and are separated from each other. I−V measurements of individual MWNTs indicate that they are metallic tubes with good electrical contact with the underlying metal electrode.[5,6] The as-polished samples show CNTs protruding above the SiO_2 matrix by about 30−50 nm due to their high mechanical resilience.[5,6] We employ EC etching to shorten and level them to the same plane as the SiO_2 matrix, exposing minimum CNT surface area.[15] The PECVD grown MWNTs have bamboo-like structure with a series of closed shells along the tube,[16] which seal off most of the hollow channel, leaving only the very end accessible by electrolytes. EC measurements are carried out in a three-electrode configuration by sealing the CNT array chip in a

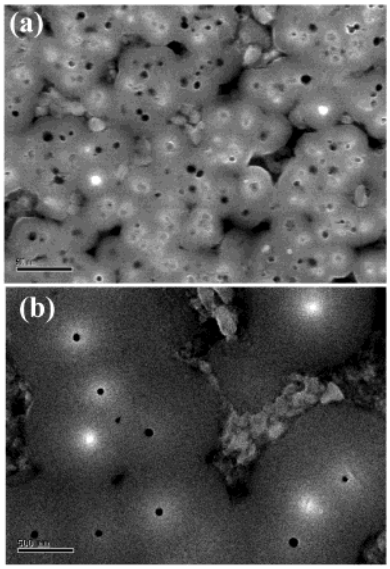

Figure 2. SEM images of two 1 × 1 cm^2 electrodes fabricated from the forest-like MWNT arrays with (a) high density and (b) low density. The average tube−tube spacing is about 280 nm and 1.5 μm, respectively. The scalebars are 500 nm. Nearly half of the CNTs in the high-density sample show dark tips slightly protruding above the SiO_2 matrix surface but wrapped with a layer of SiO_2 showing brighter contrast. Other CNTs show deep dark dots corresponding to tips shortened below the SiO_2 surface by electrochemical etching. Some deep voids between the SiO_2 grains are shown in both images.

TEFLON cell using a 3 mm i.d. O-ring. A Pt coil and a saturated calomel electrode (SCE) are used as the counter and reference electrodes, respectively.

For ease of experiment, forest-like MWNT arrays grown on 1 × 1 cm^2 Cr-covered Si substrates were used to systematically study the electrochemical properties of the CNT nanoelctrode array. Such electrodes are robust and can be easily regenerated for many experiments by brief polishing. The microarray electrode as shown in Figure 1a was confirmed to show similar properties with the macrosized CNT nanoelectrode array. Figure 2 shows SEM images obtained with two of such macrosized electrodes with very different densities at ∼3.0 × 10^9 and ∼1 × 10^8 CNTs/cm^2, i.e., averaged tube−tube spacings of 280 nm and 1.5 μm, respectively. The diameter of the MWNTs is about 100 nm.

Figure 3a,b shows the cyclic voltammetry (CV) measurements in 1.0 mM $K_4Fe(CN)_6$ and 1.0 M KCl with the two CNT array electrodes shown in Figure 2, respectively. The CV curve of the high-density array (Figure 3a) is similar to a solid macroelectrode due to the heavy overlap of the diffusion layer from each CNT electrode. The peak separation is about 96 mV, indicating that the reaction is quasi-reversible at the CNT electrode, similar to the carefully prepared conventional carbon electrodes.[12] The CV feature dramatically changes to a sigmoidal steady-state curve with the low-density sample (Figure 3b), indicating that CNTs approach to independent nanoelectrodes as they are separated enough.

The high-density nanoelectrode array can be used for highly sensitive detection of redox species in bulk solutions as demonstrated with nanoelectrode ensembles of similar

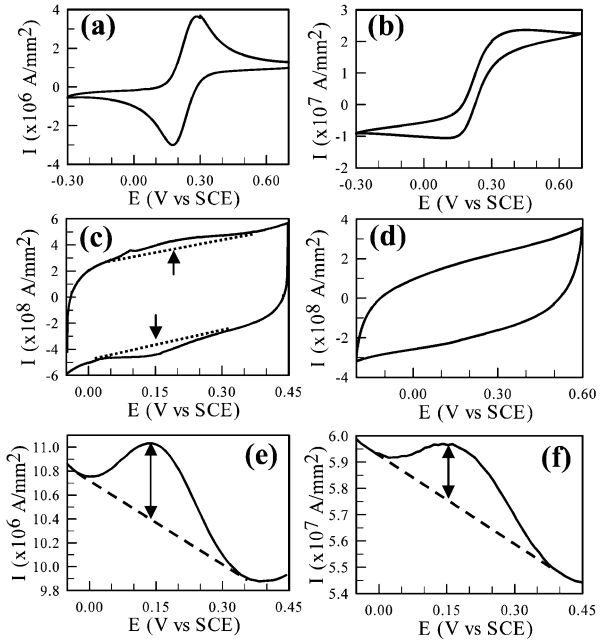

Figure 3. (a) and (b) CV measurements in 1 mM $K_4Fe(CN)_6$ and 1.0 M KCl; (c) and (d) CV measurements of Fc derivative functionalized MWNT array electrodes in 1.0 M KCl solution; and (e) and (f) ACV measurements at 50 Hz and an amplitude of 50 mV on the staircase DC ramp from 0.55 to 1.20 V. (a), (c), and (e) are measured with the high-density CNT array electrode and (b), (d), and (f) are measured with the low-density one, respectively. All CV measurements are taken with a scan rate of 20 mV/s. The arrows indicate the position of the redox waves of the Fc derivative functionalized on the CNT array electrode. The dotted lines and dash lines indicate the baselines of the background current.

density fabricated by filling nanochannels in filtration membranes.[17] In this work, we are interested in using the low-density array for ultrasensitive detection of surface-immobilized redox species. Since EC-etched CNT ends are dominated by carboxylic groups,[12,15] a ferrocene (Fc) derivative, $Fc(CH_2)_2NH_2$, can be selectively functionalized at the tube ends through amide bonds facilitated by the coupling reagents dicyclohexylcarbodiimide (DCC) and *N*-hydroxysuccinimide (NHS)[18] as illustrated in Scheme 1a. Figure 3c,d shows CV curves of the two CNT array electrodes (as shown in Figure 2) after functionalization with the Fc derivative, respectively. For the high-density sample (Figure 3c), a pair of waves can be seen centered around 0.16 V (indicated by the arrows), while it is almost only a flat background in Figure 3d with the low-density sample. The peak separation is about 30 ± 10 mV in Figure 3c, indicating a quasi-reversible surface adsorbed process consistent with the nature of the electrode indicated by CV in $K_4Fe(CN)_6$ solution.

Since each CNT is separated from others, the CNT nanoelectrode array presents a reduced cell time constant, i.e., a smaller RC factor, which is proportional to the radius of individual electrodes.[19] Thus fast electrochemical techniques such as AC voltammetry (ACV) and differential pulse voltammetry can be applied to improve the sensitivity. Here, a sinusoidal AC wave is superimposed on the slow varying staircase DC potential ramp used in normal CV so that multiple electron transfer can occur between a redox species

Scheme 1. (a) The Functionalization Process of the Amine-Terminated Ferrocene Derivative to CNT Ends by Carbodiimide Chemistry and (b) the Schematic Mechanism of $Ru(bpy)_3^{2+}$ Mediated Guanine Oxidation

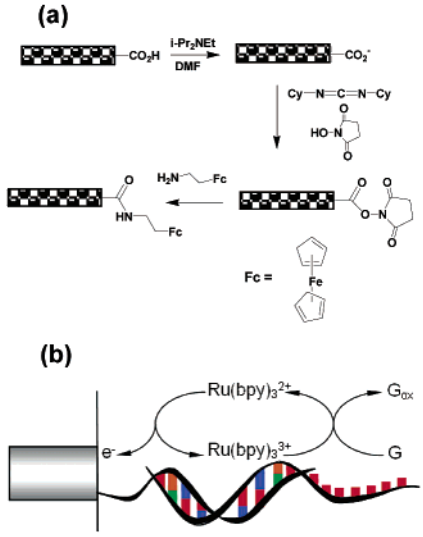

and the electrode, resulting in a much higher signal.[20] Figure 3e,f shows very similar ACV curves in 1.0 M KCl obtained with the two CNT array electrodes functionalized with Fc, respectively. Clearly, a peak corresponding to the faradaic signal is now observed at ~0.16 V with both samples. The backgrounds are stable and can be fitted with linear curves indicated by the dashed lines. The extracted peak height is proportional to the number of $Fc(CH_2)_2NH_2$ molecules on the electrode surface. The high-density sample in Figure 3e shows a peak height about 29 times of that of the low-density sample, i.e., linearly scaling with the CNT density. The baseline increases by about 18 times, slightly less than the ratio of CNT densities.

Similar carbodiimide chemistry can be applied to functionalize primary amine-terminated oligonucleotides using water soluble coupling reagents 1-ethyl-3(3-dimethyl aminopropyl carbodiimide hydrochloride (EDC) and *N*-hydroxysulfo-succinimide (sulfo-NHS).[21] We repeated the coupling chemistry as reported before[21] to functionalize the high-density CNT array electrode with 10 bp polyC probes and then hybridized with 20 bp polyG targets. The small guanine oxidation current, however, cannot be resolved by direct CV measurements due to the high exponential background current at potentials above +0.90 V, presumably due to carbon oxidation and/or water electrolysis. This is why only a few materials with wide potential windows such as carbon and indium tin oxide[7] can be used as electrodes for guanine oxidation which occurs at a high potential (~1.05 V). However, $Ru(bpy)_3^{2+}$ mediators can be employed to gain amplified signal for DNA detection as illustrated in Scheme 1b based on an electrocatalytic mechanism.[7]

Figure 4a shows three consecutive CV scans in 5 mM $Ru(bpy)_3^{2+}$ in 0.20 M NaOAc buffer solutions (pH = 4.8) after hybridizing the 20 bp polyG targets on the high-density CNT array electrode. Clearly, the oxidation wave of $Ru(bpy)_3^{2+}$ is now observed at about 1.05 V superimposed on the

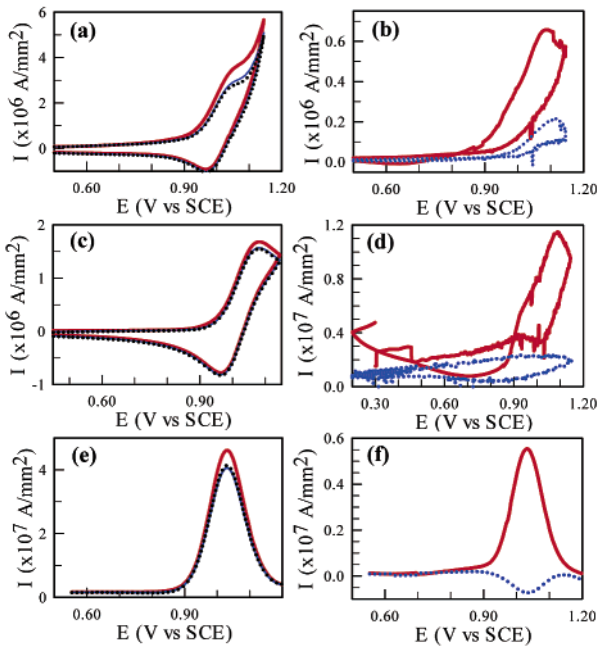

Figure 4. Three consecutive CV measurements of (a) the high-density CNT array electrode functionalized with 10 bp polyC and hybridized with 20 bp polyG, and three consecutive (c) CV and (e) ACV measurements of the low-density CNT array electrode functionalized with oligonucleotide probes with the sequence [Cy3]-5′-CTIIATTTCICAIITCCT-3′[AmC7-Q] and hybridized with oligonucleotide targets with the sequence [Cy5]5′-AGGACCTGCGAAATCCAGGGGGGGGGGG-3′, respectively. The red, blue, and black dotted lines correspond to the first, second, and third scan, respectively. All measurements are carried out in 5 mM $Ru(bpy)_3^{2+}$ in 0.20 M NaOAC supporting electrolyte (pH = 4.8). The CVs are taken at 20 mV/s and the ACVs are taken with an AC sinusoidal wave of 10 Hz and 25 mV amplitude on top of a staircase DC ramp. (b), (d), and (f) are the difference between the first and second scans (red line), and between the second and third scans (blue dotted line) corresponding to (a), (c), and (e), respectively. The positive peaks in differential curves correspond to the increase in $Ru(bpy)_3^{2+}$ oxidation signal.

exponential background. The $Ru(bpy)_3^{2+}$ oxidation current is higher in the first scan due to the electrocatalytic factor by guanine near the electrode surface.[7] Since guanine bases are irreversibly oxidized in the first scan, the $Ru(bpy)_3^{2+}$ oxidation current in consecutive scans decreases to almost a constant level corresponding to the clean electrodes.[7] This is clearly indicated by the differential curves in Figure 4b corresponding to the first scan subtracting the second scan (red line) and the second scan subtracting the third scan (blue dotted line), respectively. The positive peak in the differential curve is mainly associated with the amplification effect by guanine bases brought to the surface through hybridization. The CV measurements confirm that the guanine-mediated $Ru(bpy)_3^{2+}$ oxidation can be applied to the CNT array platform. However, our attempts for ACV with the high-density sample based on this mechanism did not give consistent results.

To explore our goal for ultrasensitive detection of biologically relevant DNA molecules using such CNT array electrodes, a probe [Cy3]5′-CTIIATTTCICAIITCCT-3′-[AmC7-Q] and a target [Cy5]5′-AGGACCTGCGAAATC-CAGGGGGGGGGGG-3′ are used, which are related to the wild-type allele (Arg1443stop) of BRCA1 gene.[22] A 10 bp polyG is attached to the target sequence as the signal moiety and the guanine bases in the probe are replaced with inosine to ensure no guanine contribution from the probe. Fluorescence images of Cy3 and Cy5 labels are taken with a laser scanner after each step of functionalization, hybridization, and washing to confirm the attachment (as shown in Figure 5a,b). The low-density CNT array is desired so that the detection limit can be lowered. Such efforts have produced excellent results and show great potential for ultrasensitive DNA detection.

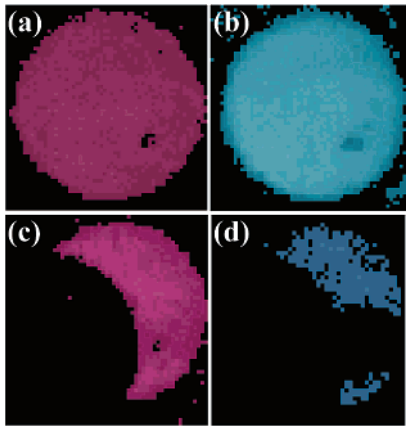

Figure 5. Fluorescence images of (a) Cy3 and (b) Cy5 at a spot on the high-density CNT array electrode functionalized with Cy3 labeled oligonucleotide probes and hybridized with Cy5 labeled oligonucleotide targets. Panels (c) and (d) are the fluorescence images of Cy3 and Cy5, respectively, at the same spot after electrochemical measurements. The O-ring is deliberately misaligned relative to the original DNA spot during the electrochemical experiment to show the difference inside and outside the EC cell. DNA molecules inside the cell (at the lower left corners) are electrochemically removed when the potential is scanned over 0.90 V, leaving the half-moon shaped DNA spot corresponding to the molecules outside the EC cell.

Figure 4c shows three consecutive CV scans in 5 mM $Ru(bpy)_3^{2+}$ in 0.20 M NaOAc buffer solutions (pH = 4.8) after hybridizing the polyG tagged BRCA1 targets on the low-density CNT array electrode functionalized with the oligonucleotide probes. Clear peaks corresponding to $Ru(bpy)_3^{2+}$ oxidation are observed at 1.05 V, with the first scan clearly higher than the second. The exponential background is much less prominent than that of the high-density sample. Scans after the second one show almost identical curves with little decrease each time. The differential curves between consecutive scans in Figure 4d are consistent with the high-density sample but much smaller. Generally, we found that these CV measurements can give qualitative answers but are difficult to be quantified because other factors such as carbon oxidation and surface changes are mixed with the guanine contribution in the first scan and sometimes even in subsequent scans, resulting in a positive differential peak similar to the dotted line in Figure 4b, even when using a clean CNT array electrode.

However, the ACV works very well with the low-density CNT array electrode. Figure 4e shows three consecutive

ACV scans in 5 mM $Ru(bpy)_3^{2+}$ in 0.20 M NaOAc buffer solutions with the BRCA1 targets on the low-density CNT array electrode. The AC current is measured by applying a sinusoidal wave of 10 Hz frequency and 25 mV amplitude on a staircase potential ramp. Well-defined peaks are observed around 1.04 V, with the first scan clearly higher than the almost superimposed subsequent scans. The background is almost a flat line at zero. As shown in Figure 4f, subtracting the second scan from the first one gives a well-defined positive peak (red line), while subtracting the third scan from the second gives a small negative peak (blue dotted line) serving as an unambiguous negative control. A clean electrode normally gives similar small negative peak in the differential curve. Interestingly, the unstable exponential background current is filtered out by the ACV, and only the Faradaic current associated with the $Ru(bpy)_3^{2+}$ oxidation is measured. The high quality of the data indicates that there is still plenty of room to lower the detection limit of target DNAs.

Generally, EC measurements can be accurately quantified, particularly with the normal CV measurements. The integrated peak area of Fc redox waves in CV obtained with the high-density sample (Figure 3c) corresponds to $\sim 2.6 \times 10^{11}$ Fc/mm^2 on the electrode, i.e., ~9000 Fc per CNT (~100 nm diameter) and ~90 Å^2/Fc. The high number of Fc per CNT is likely because some molecules are functionalized at the sidewall of the protruding tubes, particularly since the CNTs in our study have bamboo-like defective fiber structure. In any case, it is certain that the functionalization efficiency is high enough. The peak height in ACV is also proportional to the number of immobilized molecules but the absolute number is not as reliable due to the dependence of the current on the AC amplitude and frequency. For example, about 3.7×10^{10} Fc/mm^2 is calculated from the peak height of ACV data obtained with the high-density sample using the formula in ref 20, which is lower than the value of 2.6×10^{11} Fc/mm^2 derived from CV. The quasi-reversible nature of the CNT array electrode may make the deviation even bigger. The number of Fc molecules immobilized on the low-density sample is not directly measurable by normal CV. However, it can be calculated as $\sim 8.7 \times 10^9$ Fc/mm^2 by scaling the CV-based value of the high-density array with the ratio of the peak heights in corresponding ACV measurements. For a 20×20 μm^2 electrode, this gives a sensitivity of about 3.5×10^6 Fc molecules easily measurable with ACV.

For DNA-functionalized sample, it is not straightforward to estimate the exact sensitivity due to the complication of amplification mechanism using $Ru(bpy)_3^{2+}$ mediators. However, we can deduct the upper limit of the number of target DNAs based on the value of Fc on the low-density sample to show our sensitivity. Assuming that the functionalization efficiency for DNA probes is the same as the Fc derivative and the hybridization yield is 100%, 3.5×10^6 DNA target molecules (~6 attomoles) are detected based on the results shown in Figure 4e,f. These assumptions, however, are likely much higher than the actual values. Therefore, the number of DNA targets could be orders of magnitude below one attomole. We are currently exploring how to directly quantify the ACV results of the amplified DNA detection. Further optimization of the system is possible by reducing the number of CNTs on each electrode as well as adapting phase-sensitive ACV techniques to discriminate the faradaic signal from the capacitive background at proper phases.[23] In practical diagnosis, the target DNA consists of hundreds of guanine bases as active signal moieties giving a much higher signal. Thus the detection limit could be reduced well below one attomole.

The selective binding of DNA to CNTs is an important feature in our system, which enables us to lower the detection limit by reducing available CNT sites in such solid-state devices in a well-controlled way. The probe density can be fabricated precisely using lithographic techniques comparing to other approaches using mixed self-assembled monolayers whose properties strongly depend on uncontrollable defects.[3,4,8] The strong covalent binding to carbon atoms also sustains rigorous washing steps using 3×SSC, 2×SSC with 0.1% SDS, and 1×SSC, respectively, at 40 °C for 15 min after each probe functionalization and target hybridization process to get rid of the nonspecifically bound DNA molecules, which is critical for obtaining reliable EC data. If the potential in EC measurements go over 0.90 V, we found that DNA molecules can be detached from the surface, presumably due to the oxidation reaction which etches away some carbon atoms at the CNT tip. Figure 5c,d shows the fluorescence image of Cy3 and Cy5 after EC experiments with the O-ring deliberately partially misaligned on the originally functionalized and hybridized spot (shown in Figure 5a,b). Clearly, DNA molecules inside the cell are removed from the CNT ends, while most of those outside the cell still remain on the surface. This confirms that DNA molecules are indeed specifically bound to CNTs rather than physisorbed on SiO_2 surface.

In summary, we have demonstrated a new EC platform based on CNT nanoelectrode array for ultrasensitive chemical and DNA detection. The use of aligned MWNT provides a new bottom-up scheme for fabricating reliable nanoelectrode arrays. We have studied the EC characteristics of such electrode arrays with both bulk and immobilized redox species. Combining such a nanoelectrode platform with $Ru(bpy)_3^{2+}$ mediated guanine oxidation, a detection limit lower than a few attomoles of oligonucleotide targets is achieved. The sensitivity can be further improved down to thousands of target DNAs after optimization, which could provide faster, cheaper, and simpler solutions for molecular diagnosis, particularly for early cancer detection, point-of care, and field uses. This platform may be also applicable to the detection of trace redox chemicals (such as metal ions, toxic contaminants, and neurotransmitters), immunoassay-based pathogen detection, and EC detectors in microfluidic devices.

Acknowledgment. Work by ELORET authors was supported by a NASA contract. The authors also acknowledge the support by National Cancer Institute under Unconventional Innovation Program.

References

(1) Kuhr, W. G. *Nature Biotechnol.* **2000**, *18*, 1042.
(2) Sosnowski, R. G.; Tu, E.; Butler, W. F.; O'Connell, J. P.; Heller, M. J. *Proc. Natl. Acad. Sci. U.S.A.* **1997**, *94*, 1119.
(3) Umek, R. M.; Lin, S. W.; Vielmetter, J.; Terbrueggen, R. H.; Irvine, B.; Yu, C. J.; Kayyem, J. F.; Yowanto, H.; Blackburn, G. F.; Farkas, D. H.; Chen, Y.-P. *J. Mol. Diagnosis* **2001**, *3*(2), 74.
(4) Popovich, N. D.; Thorp H. H. *Interface* **2002**, *11*(4), 30.
(5) Li, J.; Stevens, R.; Delzeit, L.; Ng, H. T.; Cassell, A.; Han, J.; Meyyappan, M. *Appl. Phys. Lett.* **2002**, *81*(5), 910.
(6) Li, J.; Ye, Q.; Cassell, A.; Ng, H. T.; Stevens, R.; Han, J.; Meyyappan, M. *Appl. Phys. Lett.*, in press.
(7) Sistare, M. F.; Holmberg, R. C.; Thorp, H. H. *J. Phys. Chem. B* **1999**, *103*, 10718.
(8) Boon, E. M.; Ceres, D. M.; Drummond, T. G.; Hill, M. G.; Barton J. K. *Nature Biotech.* **2000**, *18*, 1096.
(9) Wightman, R. M. *Anal. Chem.* **1981**, *53*, 1125A.
(10) Penner, R. M.; Heben, M. J.; Longin T. L.; Lewis, N. S. *Science* **1990**, *250*, 1118.
(11) Fan, F.-R. F.; Bard, A. J. *Science* **1995**, *267*, 871.
(12) McCreery, R. L. In *Electroanalytical Chemistry*; Bard, A. J., Ed.; Marcel Dekker: New York, 1991; ch. 17, pp 221−374.
(13) Nugent, J. M.; Santhanam, K. S. V.; Rubio, A.; Ajayan, P. M. *Nano Lett.* **2001**, *1*(2), 87.
(14) Campbell, J. K.; Sun, L.; Crooks, R. M. *J. Am. Chem. Soc.* **1999**, *121*, 3779.
(15) CV measurements of an as-polished sample in 1.0 mM $K_4Fe(CN)_6$ with 1.0 M KCl supporting electrolyte gives a pair of redox waves separated by more than 700 mV. A thermal annealing for more than 1 h in air at 250 °C followed by electrochemical etching in 1.0 M NaOH at 1.5 V for 1−2 min can dramatically reduce the peak separation to about 100 mV. The pretreated MWNT nanoelectrode array remains active for days and can be repeatedly used. The pretreatment converts most of the functional groups at the CNT ends to −COOH and −OH as described in ref 12.
(16) Delzeit, L.; McAninch, I.; Cruden, B. A.; Hash, D.; Chen, B.; Han J.; Meyyappan, M. *J. Appl. Phys.* **2002**, *91*, 6027.
(17) Menon, V. P.; Martin, C. R. *Anal. Chem.* **1995**, *67*, 1920.
(18) Hermanson, G. T. *Bioconjugate Techniques*; Academic Press: New York, 1996; pp 178.
(19) Bard, A. J.; Faulkner, L. R. *Electrochemical Methods: Fundamentals and Applications*, 2nd ed.; Wiley: New York, 2001; pp 216−218.
(20) Creager, S.; Yu, C. J.; Bamdad, C.; O'Connor, S.; Maclean, T.; Lam, E.; Chong, Y.; Olsen, G. T.; Luo, J.; Gozin, M.; Kayyem, J. F. *J. Am. Chem. Soc.* **1999**, *121*, 1059.
(21) Nguyen, C. V.; Delzeit, L.; Cassell, A. M.; Li, J.; Han, J.; Meyyappan, M. *Nano Lett.* **2002**, *2*(10), 1079.
(22) Miki, Y.; Swensen, J.; Shattuck-Eidens, D.; Futreal, P. A.; Harshman K.; Tavtigian, S.; Liu, Q.; Cochran, C.; Bennett, L. M.; Ding, W. *Science* **1994**, *266*, 66.
(23) Bond, A. M. *Modern Polarographic Methods in Analytical Chemistry*; Marcel Dekker: New York, 1980.

NL0340677